ORIGINAL

Experimental investigation of the Cu/R141b nanofluids on the evaporation/boiling heat transfer characteristics for surface with capillary micro-channels

Yanhua Diao · Yan Liu · Rui Wang · Yaohua Zhao · Lei Guo

Abstract An experimental study was conducted to investigate the heat transfer characteristic of a vertical copper plate with rectangular micro-channels. In this research, Cu/R141b nanofluids were used as the working fluid. Three different volume concentrations—0.001, 0.01, and 0.1 %—of Cu nanoparticles with an average diameter of 20 nm dispersed in R141b were prepared. Experiments were performed to measure thermal resistance of the microchannel surface under a steady operating pressure range of 0.86×10^5 Pa to 2×10^5 Pa. Thermal resistance weakened with addition of nanoparticles into the base fluid. The maximum reduction effect of the thermal resistance was 50 %, which corresponds to 0.01 % volume concentration of nanofluid at low operating pressure. The operating pressure significantly affects thermal performance of the microchannel surface. This paper also studied heat transfer characteristics for a Cu nanoparticle-coated surface with rectangular microchannels, which were produced by heating in different volume concentrations from 0.001 to 0.1 %. Nanoparticle layer on the micro-channel surface is responsible for enhanced heat transfer of nanofluids with 0.001 and 0.01 % volume concentrations.

List of symbols

q	Heat flux (W m^{-2})
l	Distance between two thermocouples (m)
R	Thermal resistance (m^2 K W^{-1})

T_t	Temperature of the copper plate with micro-channels (K)
T_s	Saturation temperature of the working fluid (K)
T_1, T_2, T_3, T_4	Temperature of the copper heater (K)

Greek symbol

λ	Thermal conductivity of the pure copper (W m^{-2} K^{-1})

1 Introduction

Heat pipes and vapor chambers perform excellently in efficient heat transport because of transferred energy via liquid–vapor phase change of the working fluid. Thus, the choice of the working fluid is vital in thermal performance of heat pipes.

Nanofluids are a new type of engineered heat transfer fluid developed by Argonne National Laboratory, USA. They are generated by suspending nanometer-sized metallic or nonmetallic particles in base fluids, such as water, engine oil, and ethylene glycol [1]. Many researchers have investigated thermal conductivity [2–9], convective heat transfer, and pool boiling heat transfer characteristics of nanofluids [10–24]. Nanoparticles, such as Ag, CuO, Al$_2$O$_3$, diamond, iron oxide, and Au, have been used to study the influence of nanofluids on thermal performance of micro-grooved heat pipes [25–28], mesh wicked heat pipes [29–31], sintered metal heat pipes [32], thermosyphons [33–35], and oscillating heat pipes [36–38].

Liu et al. [25] investigated the effects of aqueous Cu nanofluids with different nanoparticles on the thermal performance of a cylindrical micro-grooved heat pipe under different operating pressures. The addition of Cu and CuO nanoparticles to the base fluid can improve the

Y. Diao (✉) · Y. Liu · R. Wang · Y. Zhao · L. Guo
The Department of Building Environment and Facility Engineering, The College of Architecture and Civil Engineering, Beijing University of Technology, Beijing, China
e-mail: diaoyanhua@bjut.edu.cn

thermal performance of the heat pipe. By contrast, the addition of SiO nanoparticles deteriorates heat transfer performance. The heat transfer mechanism was presented as follows: (1) Increased effective thermal conductivity of the nanofluid can enhance conductive heat transfer; (2) Decreased solid–liquid contact angle between the nanofluid and the heated surface can increase capillary force and stretch liquid film in the grooves; (3) Random collision of nanoparticles in the base fluid (Brownian motion), which is a nanoscale effect, can enhance convection; (4) The last aspect of the heat transfer mechanism is attributed to the coating layer formed on the heated surface during the heating process.

Tsai et al. [30] studied the thermal performance of a conventional circular meshed heat pipe by using an aqueous solution of gold nanoparticles. The thermal resistance of the heat pipe that used nanofluids is 37 % lower than that which used deionized water.

Chen et al. [31] studied the thermal performance of an axially flat mesh wicked heat pipe by using silver nanoparticle suspensions. The total resistance of the heat pipe that used nanoparticle suspensions is lower than that of the heat pipe that used DI water.

Kang et al. [32] used water/Ag nanofluids as the working fluid for a conventional sintered circular heat pipe with a 1 mm wick thickness. Nanoparticles with 10 and 30 nm diameters were used. Accordingly, the increase in the difference in wall temperature for heat pipe with nanofluid is smaller than that for a heat pipe filled with pure water under various heat loads.

Noie et al. [34] employed water/Al$_2$O$_3$ nanoparticle suspensions as the working fluid in a thermosyphon. For different input powers, the efficiency of the thermosyphon increased up to 14.7 % when Al$_2$O$_3$/water nanofluid was used instead of pure water.

Huminic et al. [35] also studied the heat transfer characteristic of a thermosyphon with iron oxide/water as the working fluid. Nanoparticles significantly influenced the enhancement of the heat transfer characteristic of the thermosyphon.

Qu et al. [36] experimented on the thermal performance of an oscillating heat pipe charged with Al$_2$O$_3$/water nanofluid. Alumina nanofluids significantly improved the thermal performance of the oscillating heat pipe. The change of surface condition at the evaporator due to the settlement of the nanoparticle was the major factor in the enhanced thermal performance of the oscillating heat pipe.

Ma et al. [38] investigated a nanofluid oscillating heat pipe to determine the effect of nanofluids on transport capability. The heat transport capability of the oscillating heat pipe increased significantly when it was charged with nanofluid. In addition, heat transport capability depends on the operating temperature.

Do et al. [39] studied whether the enhancement of heat transfer in nanofluid heat pipes can be attributed to changes in fluid thermophysical properties and to characteristics of a heat transfer surface. They constructed two mathematical models to investigate the heat transfer characteristics of a flat microheat pipe with a grooved wick by using water-based Al$_2$O$_3$. Model I represented the heat transfer enhancement caused by changes in fluid thermophysical properties under the assumption that nanofluids in the base fluid were uniformly dispersed and suspended without any accumulation or deposition on the heat transfer surface in the evaporation region. Model II represented the enhancement of heat transfer brought about by changes in the heat transfer surface caused by nanoparticle deposition. Model II was more applicable for predicting the thermal performance of nanofluid heat pipes.

Though many studies on the heat transfer enhancement for nanofluids use as the working medium in thermosyphons have been conducted, the heat transfer enhancement mechanism by using nanofluids has not yet been rigorously investigated.

In the previous report by Diao et al. [40], the microchannel heat sink resulted in excellent thermal performance for a high-powered chip cooling application was investigated experimentally. In this study, nanofluid Cu/R141b was used as the working fluid for different volume concentrations to study the phase change heat transfer characteristic for a vertical plate with rectangular microchannels under a saturated vapor ambient at different operating pressures. A significant improvement in the heat transfer for the microchannel surface was achieved by using Cu/R141b nanofluids instead of pure R141b. Nanoparticle coverings (nano-coverings) used in enhancing heat transfer were also investigated. Nano-coverings on the evaporator surface can significantly affect heat transfer performance and are responsible for improved heat transfer of nanofluids on the plate with microchannels.

2 Nanofluid production

This study used Cu with an average diameter of 20 nm as nanoparticles. Cu/R141b nanofluids were produced via two-step method. Dried Cu nanoparticles were dispersed directly into R141b. Cu nanoparticles with an average diameter of 20 nm were purchased from a commercial manufacturer. To prevent formation of nanoparticle agglomerates in Cu–R141b mixture and to generate a stable nanofluid, an ample amount of dispersant SDBS was added to the base fluids, and solid–liquid mixtures were oscillated by using an ultrasonic cleaner for more than 10 h. The amount of the SDBS is twice that of nanoparticles for different nanoparticle volume concentrations.
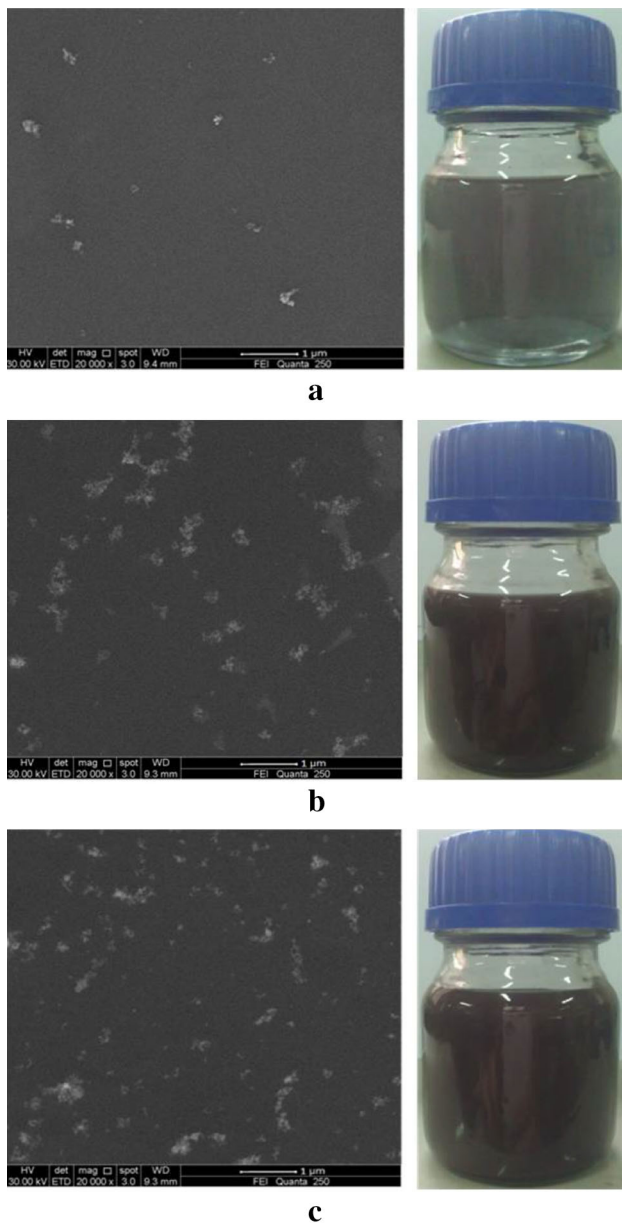
Fig. 1 SEM images of Cu nanoparticles. **a** 0.001 % volume concentration, **b** 0.01 % volume concentration, **c** 0.1 % volume concentration

Thus, the volume concentrations of SDBS were twice that of nanoparticles. Cu/R141b nanofluids with three different volume concentrations of 0.001, 0.01, and 0.1 % were prepared for this experiment. Figure 1 shows SEM photographs of the nanofluids with different volume concentrations.

3 Experimental setup

The experimental system is illustrated in Fig. 2. It mainly consists of a test vessel, condensing system, copper bar
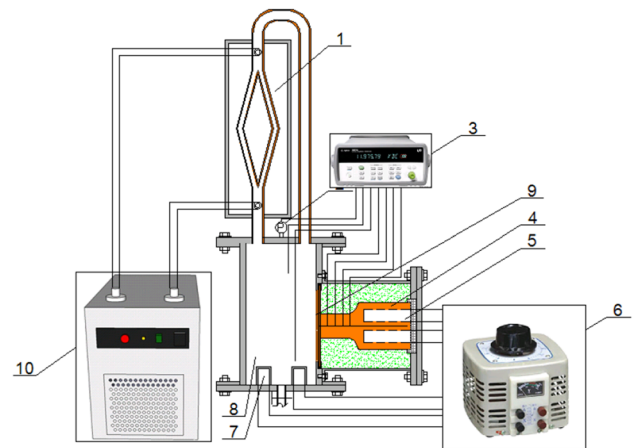

Fig. 2 Schematic of experimental apparatus. *1* condenser, *2* pressure sensor, *3* Agilent D.A. system, *4* heating block, *5* primary heater, *6* voltage regulator, *7* auxiliary heater, *8* evaporation chamber, *9* heat transfer surface, *10* refrigerator

main heater and auxiliary heaters, power supply, and a data acquisition system. The internal dimensions of the test vessel are 70 mm × 60 mm × 125 mm. Four electrical heaters were inserted in the copper bar and used for evaporation/boiling tests. A water cooling condenser was mounted on the test vessel for vapor condensing. Cooling water was circulated through the condenser at a constant velocity to remove heat then placed in a water bath with a constant temperature. The cooling water temperature was controlled precisely to maintain a constant operating pressure and temperature in the vessel for different heat flux.

Two P-100-type thermoresistances were used to measure liquid and vapor temperatures. Two auxiliary cartridge heaters were mounted at the bottom inside the test vessel to maintain the liquid and vapor at saturation temperature. A pressure transducer installed on the top plate was used to measure the operating pressure of the test vessel. A data acquisition system was used to monitor temperature readings throughout the copper block. The thermocouples readings were recorded by the multi-channel data acquisition system and the measurement readings were recorded at a frequency of 0.1 Hz. A computer was set up to record and process the experimental data.

The structure of the test heater is illustrated in Fig. 3. In this section, the locations for temperature measurement are shown. The heated surface is the top surface of a copper round-type block with a 20 mm diameter and heated by four electrical cartridge embedded heaters. The maximum power provided by all heaters could reach 1,000 W. The copper block was thermally insulated by a glass wool layer and fiber blankets.

The top surface of the copper was attached symmetrically to the plate with micro-channel. In the copper block,
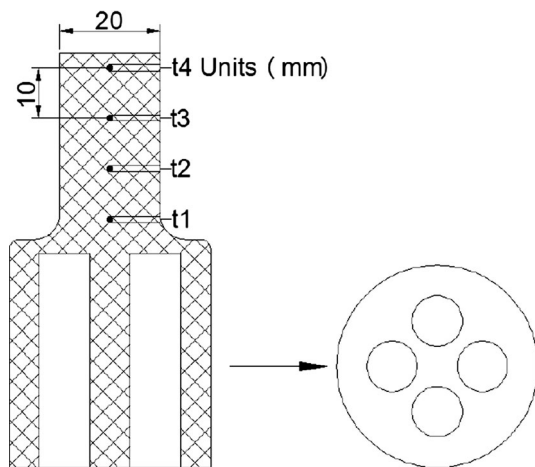
Fig. 3 Structure of heating block and arrangement of thermocouples
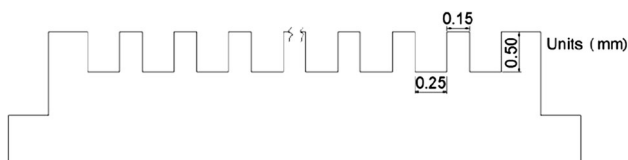

Fig. 4 Micro-channel structure

four holes, each 10 mm deep and 1 mm in diameter, were drilled into the center of the copper block at 10 mm intervals. Copper-constantan sheathed thermocouples with a diameter of 1.0 mm were embedded in each hole. With the temperature difference between thermocouples T_1 and T_2 as well as the thermal conductivity of the pure copper heating section, the steady-state 1-D axial average heat flux could be calculated. Hence, steady-state heat dissipation that results from evaporation/boiling from the micro-channel surface could be determined with high accuracy. The space between the contact surfaces was then filled with Ag thermal silicone, whose thermal conductivity is above 4.0 W m^{-1} K^{-1}.

A schematic of the micro-channel surface is shown in Fig. 4. Twenty-five micro-channels were cut into the top surface of the copper blanket with a 44 × 60 mm^2 area by using precision sawing. The test piece contains micro-channels that are 250 μm wide (W_c) and 500 μm high (d) with a 150 μm thick (p) intervening fin.

For each experimental iteration, the evaporator was filled with a pre-measured amount of working fluid. A filler tube was used after eliminating any non-condensable gases from the evaporator by using a vacuum pump. Figure 5 illustrates the arrangement of the heated area at the back of the copper plate with micro-channels. The initial liquid level in the reservoir is at the bottom edge of the heated region.
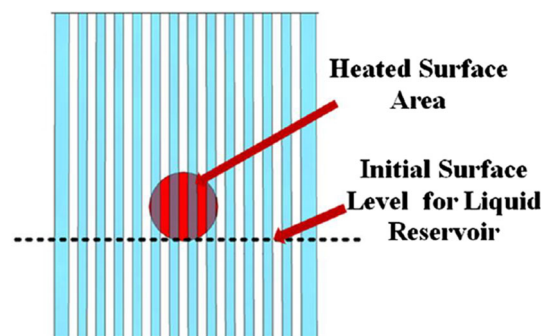

Fig. 5 Schematic of copper plate with micro-channel and heater surface with respect to the liquid reservoir
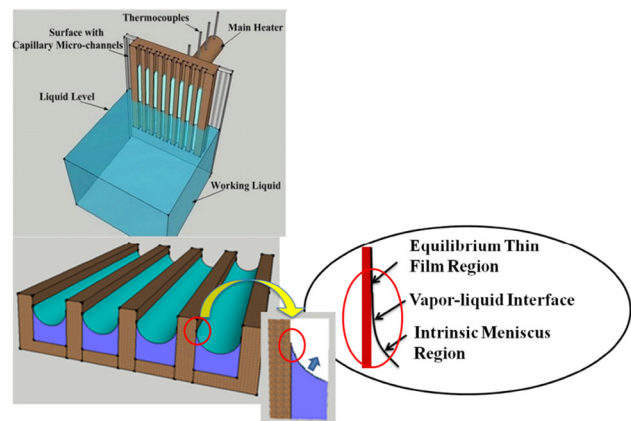

Fig. 6 Schematic of meniscus in the micro-channels

During the experiment, the working liquid was driven by capillary force into the micro-channels of the evaporator surface; phase change occurred because of input heat flux. At the surface of the micro-channels, the heat from the copper heater was absorbed by the working liquid. The vapor was condensed to release latent heat to the cooling water via convection. The condensed liquid was then drawn back to the evaporation chamber to complete a cycle. The heat transfer process mainly occurred at the liquid–vapor interface. Figure 6 shows a portion of the micro-channel that contains working liquid. Micro-channels stimulate thin liquid films and supply working liquid to the evaporating region. A concave vapor–liquid interface is formed. The curvature of the vapor–liquid interface changes as heat flux increases.

4 Experimental procedure

For each experiment, after the micro-channel surface was set, the vessel was emptied by using a vacuum pump;

Fig. 7 Relationship of heat flow density and the degree of superheat at different pressures and particle concentrations of nanofluids

a

b

c

d

e

f
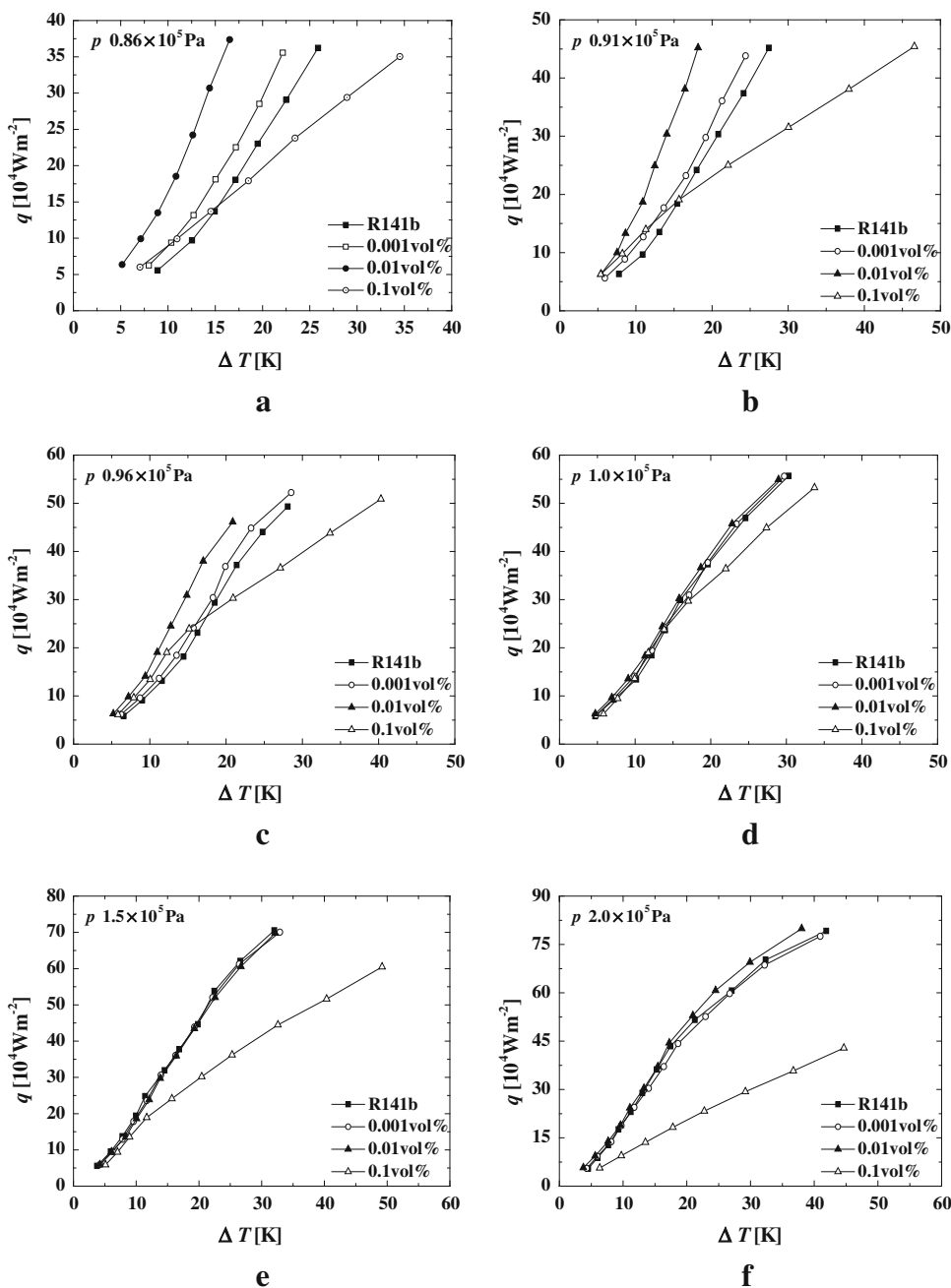
prepared nanofluid liquid was supplied into the vessel. Through the main heater, heat was supplied to the micro-channel surface. At the same time, heat input to the auxiliary heaters was adjusted to a proper value to maintain the working fluid at a saturated state. Tests were conducted after allowing the nanofluid temperature to level off at a constant temperature. During each run, power was supplied increasingly to the main heater and auxiliary heaters. In each run, the heating power increased monotonically. The heat flux q that dissipated through the evaporation plate under steady conditions could be determined by using Eq. (1)

$$q = \frac{\lambda(T_1 - T_2)}{l} \tag{1}$$

$$T_t = T_4 - q\frac{1}{\lambda} \tag{2}$$

$$R = \frac{T_t - T_s}{q} \tag{3}$$

where l is the distance between the thermocouples; T_1, T_2, T_3, and T_4 are the temperature values of the four thermocouples in the copper heater; T_t is the temperature for the back of the copper plate with micro-channels; T_s is the

Fig. 8 Relationship of thermal resistance and the degree of superheat at different pressures and particle concentrations of nanofluids
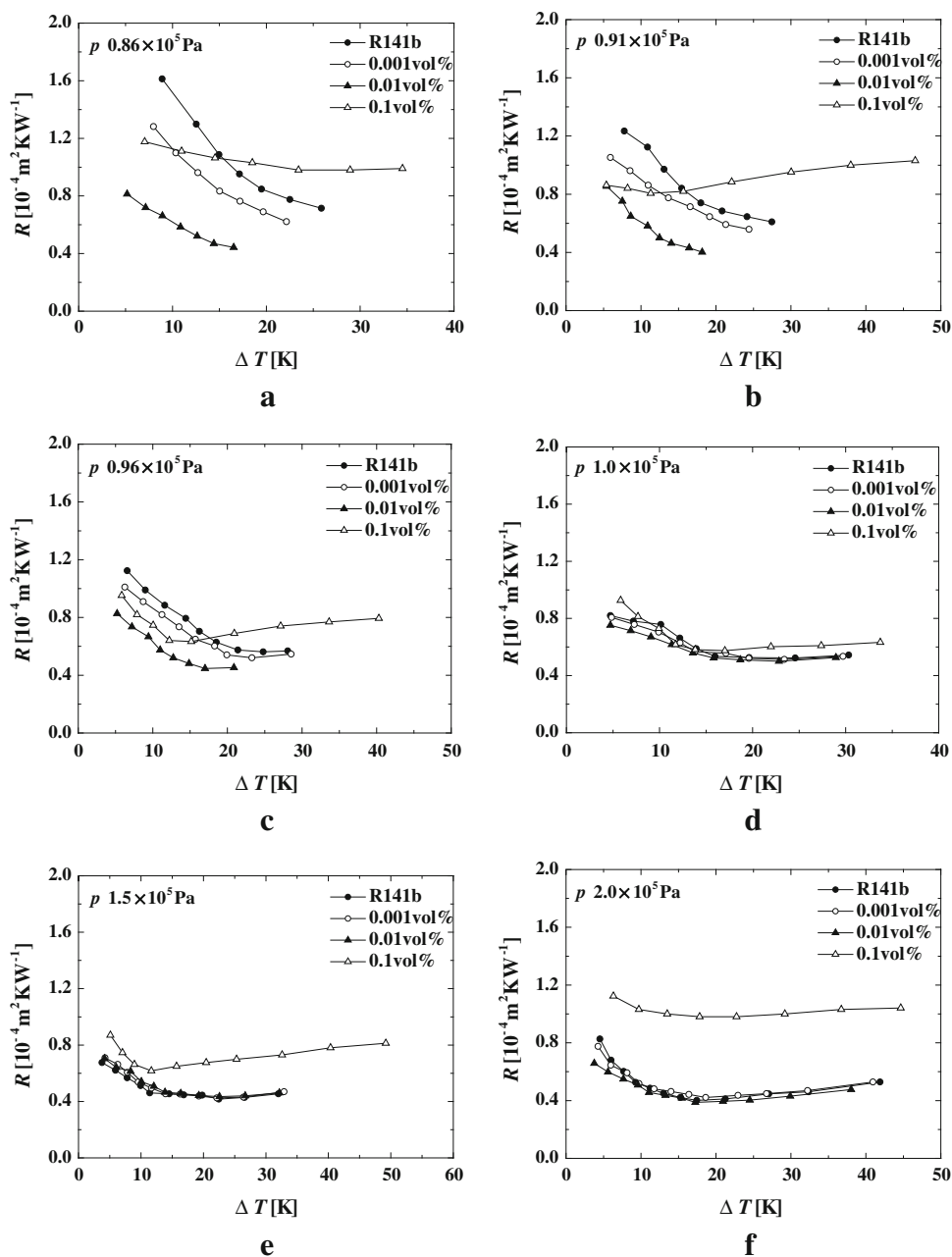
saturation temperature of the working fluid at operating pressure; R is the thermal resistance.

Uncertainties in the temperature measurements and length (width) are ± 0.1 K and 0.01 mm, respectively. The uncertainty of pressure transducer is ± 0.5 %. The evaluation of uncertainty is based on the fact that a differential change of a function can be expressed in terms of differential changes of the dependent variables [12]. The uncertainties are calculated as follows: the heat flux was estimated to be less than ± 7.22 %, and the thermal resistance is less than ± 7.17 %.

5 Results and discussion

5.1 Results of nanofluid boiling experiments

Figure 7 shows the boiling curves of the average evaporation heat flux q versus the wall superheat for Cu nanofluids with volume concentrations of 0.001, 0.01, and 0.1 % in comparison with that of pure water under six steady operation pressures.

Heat flux increases as the wall superheat increases (Fig. 7). For the boiling values of tested nanofluids with
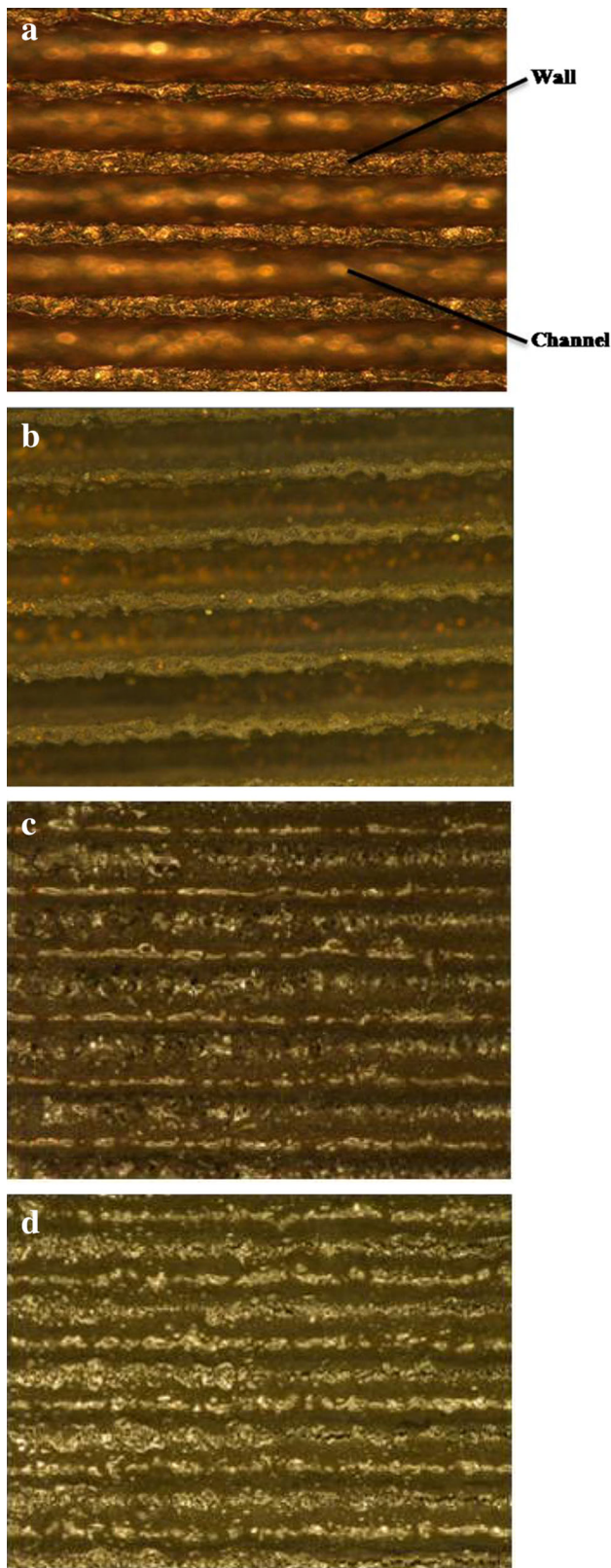
Fig. 9 Photographs of microchannel surface before and after experiment. **a** Structure of micro-channel before experiment, **b** structure of micro-channel after the experiment (0.001 % volume concentration), **c** structure of micro-channel after the experiment (0.01 % volume concentration), **d** structure of micro-channel after the experiment (0.1 % volume concentration)

that for a given wall superheat, heat flux increases as nanoparticle concentrations escalate. Figure 7a–c show that at a lower wall superheat, heat flux for the nanofluid R141b-Cu with 0.1 % volume concentration is larger than that for the pure R141b. However, at a higher superheat degree, the curve for the nanofluids with 0.1 % concentration shifts to the right. Thus, heat transfer deterioration occurred at a higher wall superheat. These results indicate that nanoparticle concentration significantly influences evaporation/boiling heat transfer at every test pressure. Figure 7d, e show that as the wall superheat increases, the curve for the nanofluid with 0.1 % volume concentration shifts to the right. This phenomenon indicates that at higher heat flux, compared with base fluid R141b, heat transfer deterioration effect occurs. Figure 7f shows that heat transfer deterioration occurs in the operating range at 2.0×10^5 Pa.

Figure 8a–c show the evaporation/boiling thermal resistance of Cu/R141b nanofluid versus the wall superheat in the 0.86×10^5 Pa to 0.96×10^5 Pa pressure range. The thermal resistance decreases as the wall superheat increases. The thermal resistance of nanofluids with 0.001 and 0.01 % concentrations for the entire range is improved at different degrees because of nanoparticles. Reduction is highly noticeable at low operating pressure. Figure 8d–f indicate that thermal resistance first decreases as wall superheat increases and reaches the lowest point, and then begins to increase with further increase of wall superheat in the 1.0×10^5 Pa to 2.0×10^5 Pa pressure range. The thermal resistance reducing effect is not obvious for nanofluids with concentrations of 0.001 and 0.01 % compared with the base fluid R141b. Figure 8f shows a clear deterioration of heat transfer effect for the nanofluid with 0.1 % concentration compared with R141b at the operating pressure of 2.0×10^5 Pa. For the tested pressures, an optimal volume concentration exists, which corresponds to the lowest reduction effect of the thermal resistance of approximately 0.001 %. Thermal resistance for R141b is 50 % of the thermal resistance of nanofluid with 0.01 % volume concentration.

The improvement in heat transfer for the nanofluids is likely due to the nanoparticle layer that formed on the microchannel surface. Compared with the clean microchannel surface, the nanoparticle layer that formed on the channel surface could extend the evaporation area to enhance evaporation heat transfer. Active nucleation site density on the nanoparticle layer may also enhance the

volume concentrations of 0.001 and 0.01 %, the boiling curves of R141b-Cu nanofluids significantly shift to the left compared with that of pure R141b. This result indicates

Fig. 10 Heat flow density and thermal resistance comparison between bare microchannel/ 0.001 vol % Cu nanofluid and 0.001 vol % coated microchannel surface/pure R141b
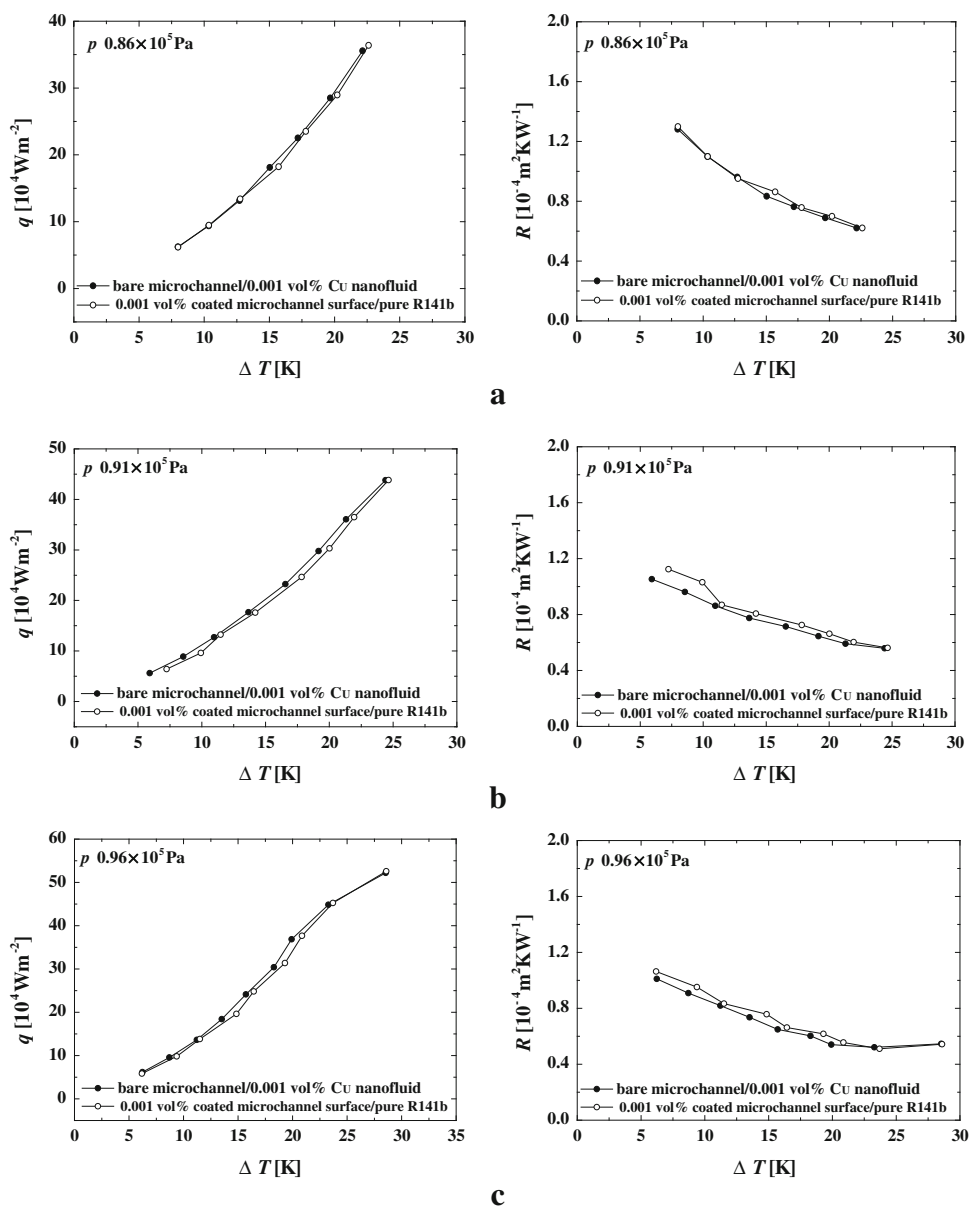
boiling transfer process in the micro-channels. The increase in the thermal resistance with improved nanoparticle concentration of 0.1 % can be attributed to the corresponding thicker nanoparticle layer, which in turn offers improved thermal resistance. As the nanoparticle deposition increases, the additional layer of nanoparticle covering increases the covering thickness. Given this phenomenon, an optimal nanofluid concentration exists in which one observes minimum thermal resistance. Results from this study indicate that the optimal nanofluid concentration is approximately 0.01 %.

Figure 9 shows pictures of the micro-channel surface captured via 3D microscopy. The pictures indicate improved deposition with increased nanoparticle concentration. A significant deposit of nanoparticles was noted on the micro-channel surface after nanofluid evaporation/boiling experiments. The degree of coverage of Cu nanoparticle deposition increases as nanoparticle concentration improves. A higher nanofluid concentration indicates thicker nanoparticle covering on the heater surface, which increases thermal resistance.

5.2 Source of nanoparticle deposition

Some researchers have studied the reason for the formation of a nanoparticle deposition layer on the heated surface. Kwark et al. [17] investigated mechanisms that may be responsible for depositing and adhering nanoparticles to
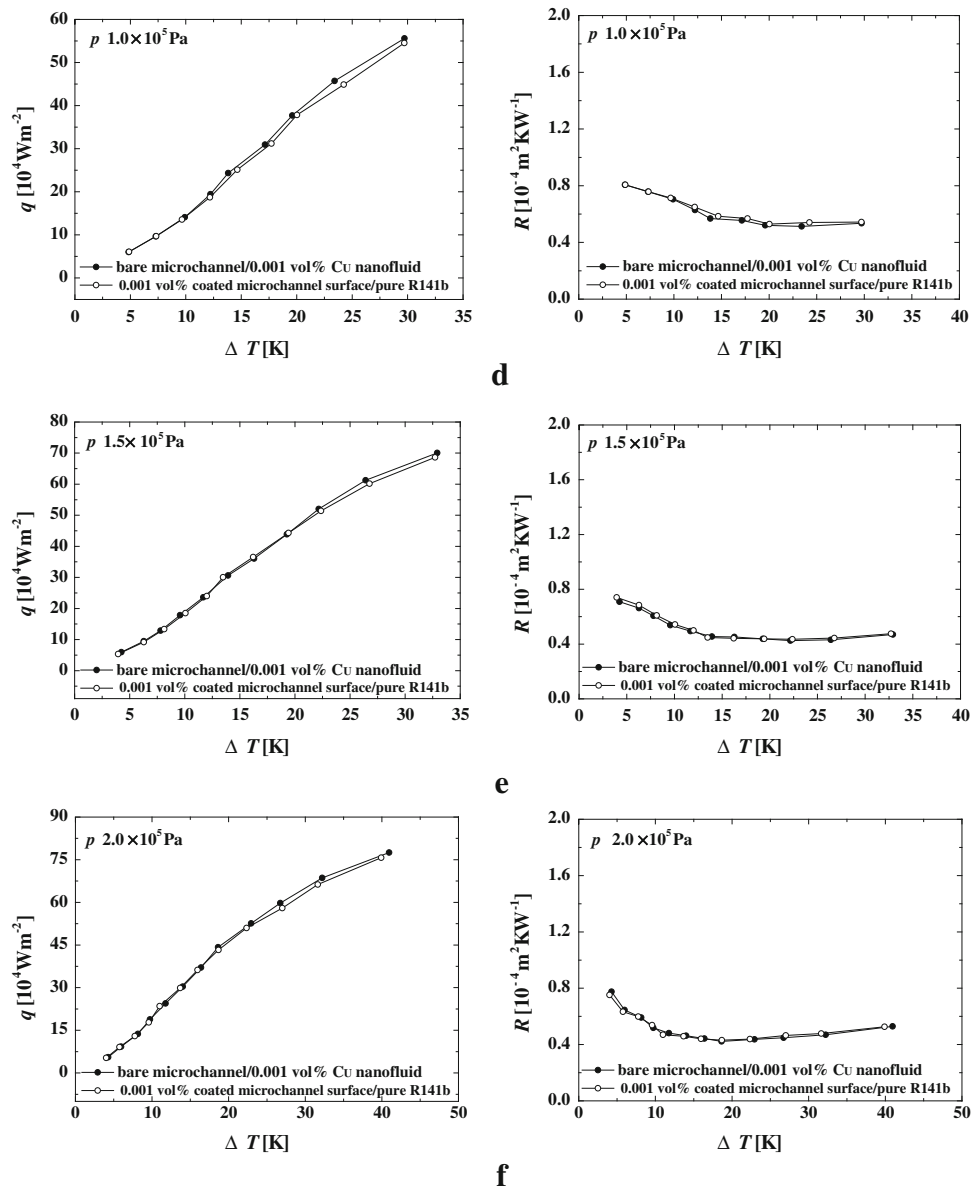
Fig. 10 continued

the heater surface during nanofluid boiling. They reported that nanofluid boiling, specifically microlayer evaporation, is responsible for the deposition and adherence of nanoparticle coatings on the heater surface. This finding is consistent with previous studies by Kwark et al. [16] and Kim et al. [19], who hypothesized that the nanoparticle coatings, which formed during nanofluid boiling, are created as the vapor bubble's microlayer evaporates. As vapor bubbles grow, the evaporating liquid leaves nanoparticles behind, which then concentrate at the base of the bubble, namely, the microlayer. As the microlayer evaporates, it leaves the nanoparticles behind, which then bond to the hot heater surface.

In the present study, two heat transfer modes can be considered: the evaporation heat transfer on the contact line (including meniscus) and the heat transfer by many micro-vapor bubbles generated in the micro-channels. Thus, the nanoparticle layer formed on the micro-channel surface is related to liquid evaporation on the contact line, and liquid evaporation beneath the bubble leaves nanoparticles behind, which then bond on the micro-channel surface.

To clarify the evaporation/boiling heat transfer mechanism for the nanofluids in the vapor chamber with rectangular micro-channels, we conducted a series of tests that used a nanoparticle-coated surface obtained by using a

Fig. 11 Heat flow density and thermal resistance comparison between bare microchannel/0.01 vol % Cu nanofluid and 0.01 vol % coated microchannel surface/pure R141b
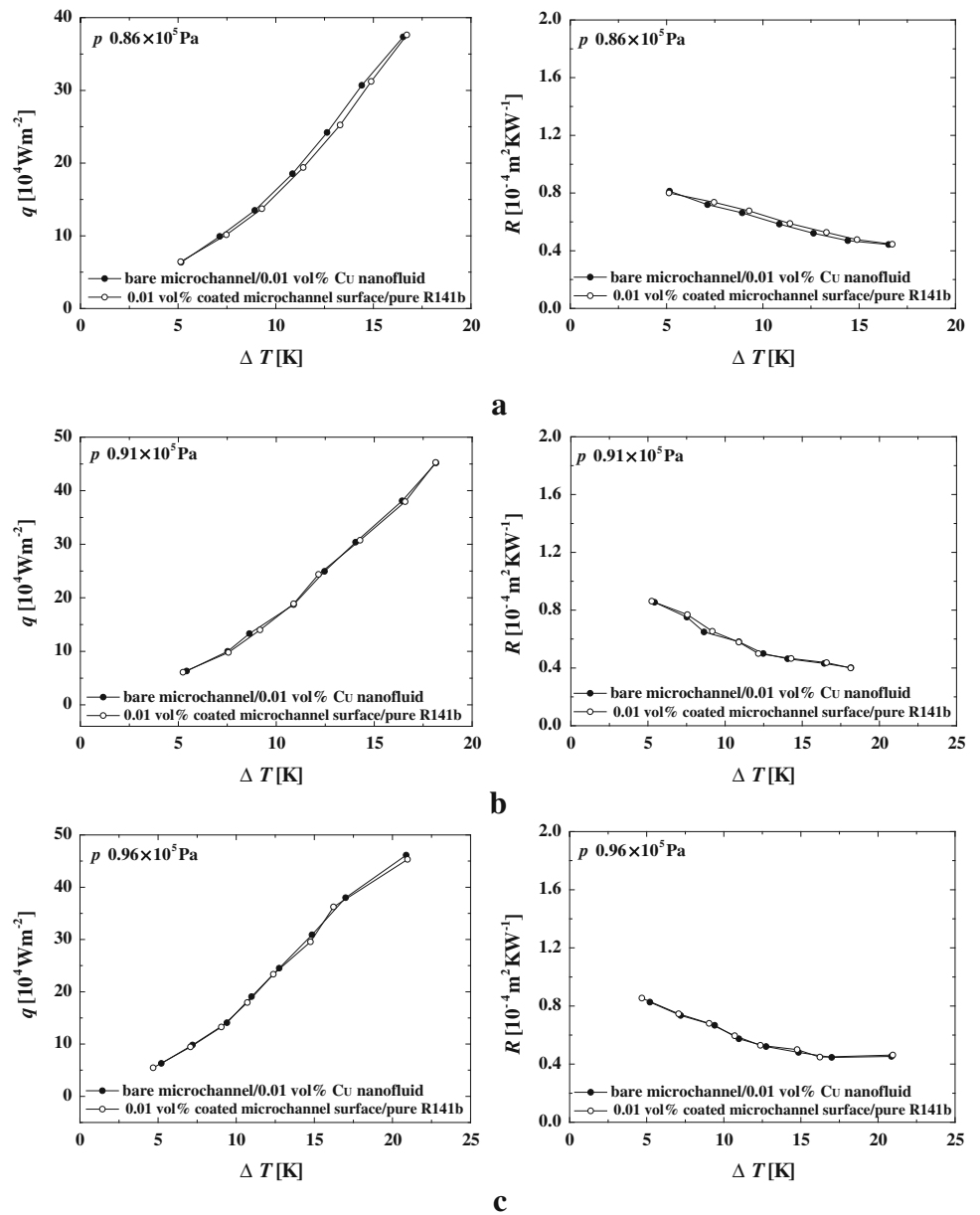
clean micro-channel surface in Cu nanofluids in pure R141b.

The nanoparticle layer accumulated on the microchannel surface in the first test. In the second test, we investigated the effect of this layers on evaporation/boiling heat transfer performance in pure R141b. As previously mentioned, these nanoparticle layers were produced during nanofluid evaporation/boiling experiments at three nanofluid concentrations of 0.001, 0.01, and 0.1 %. Thus, the nanoparticle layer created during experiments that used 0.001, 0.01, and 0.1 % nanofluid concentrations will be defined as 0.001 % nanoparticle layer, 0.01 % nanoparticle layer, and 0.1 % nanoparticle layer, respectively.

Figure 10 plots the thermal resistance versus the wall superheat for nanoparticle layer covering surface in pure R141b under different operating pressures of 1.0×10^5 Pa to 2.0×10^5 Pa. For purposes of comparison, the thermal performance against the wall superheat for clean surface in nanofluids is presented in the same figure. Figure 10a–d show that the curve for the clean surface in nanofluids almost coincides with that for the nano-covering in pure R141b at a low operating pressure of 0.86×10^5 Pa to 0.96×10^5 Pa. Figure 10e, f show the discrepancy between the two curves at a higher operating pressure of 1.0×10^5 Pa to 2.0×10^5 Pa compared with that for the lower operating pressure. Figure 11 illustrates the thermal
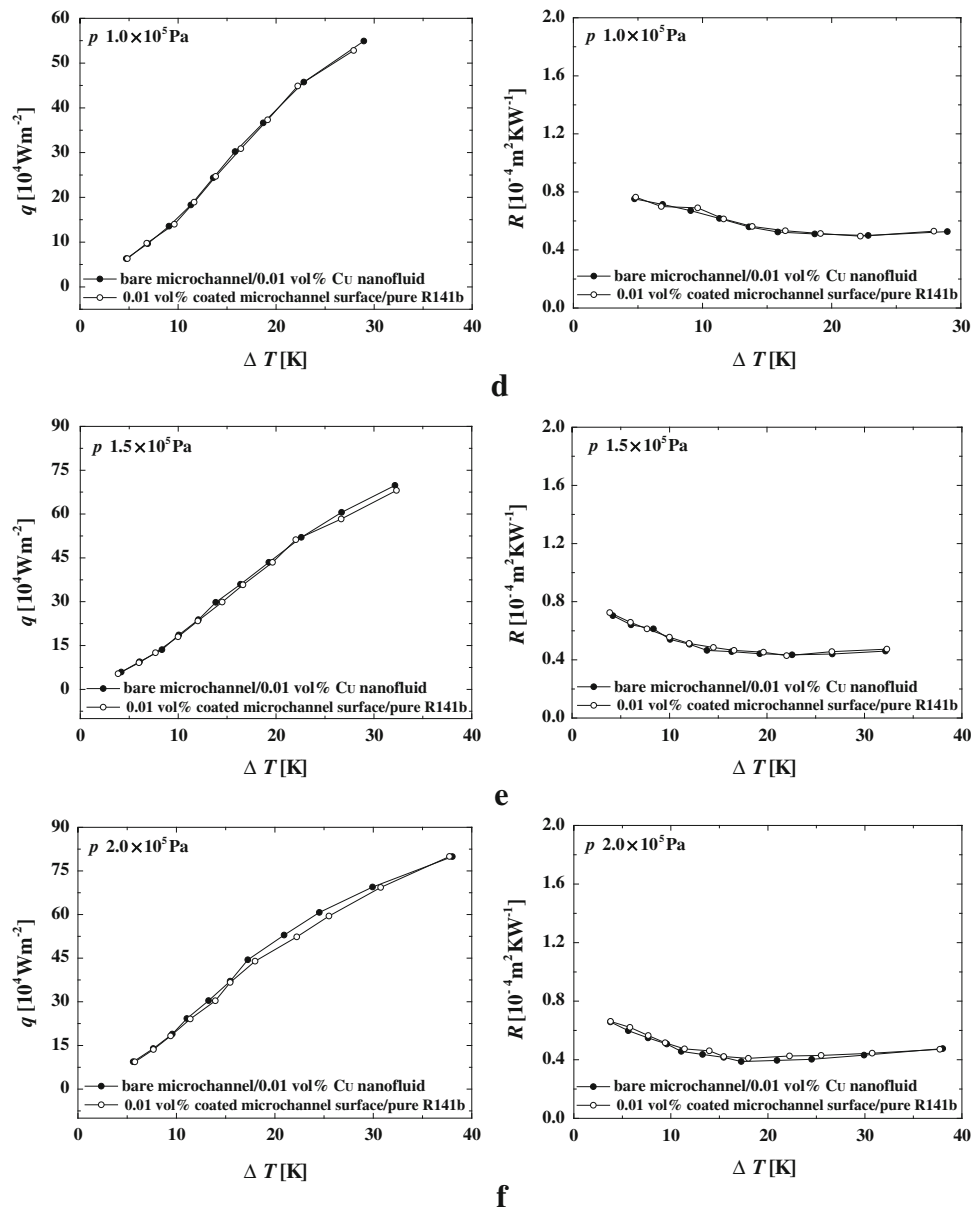
Fig. 11 continued

resistance versus the wall superheat for nanoparticle layer covering surface in pure R141b and for clean surface in nanofluids with the 0.01 % nanofluid concentration. Figure 11 shows the same trend as Fig. 10. The nanoparticle layer produced by using 0.001 and 0.01 % nanofluids produce almost the same heat transfer enhancement as nanofluids. Figure 12a–d show that for nanofluids with a higher concentration of 0.1 %, the result is a relatively large difference of thermal resistance values for the clean heater tested in nanofluids and the 0.1 % nanoparticle-coated heater tested in pure R141b for all test operating pressures. This finding means that the 0.1 % nano-covering is thicker. Thus, any nano-covering that is easily removed during evaporation/boiling has a distinct effect on heat transfer.

When the nanoparticle -coated micro-channel surface was tested in pure R141b, evaporation/boiling on the micro-channel surface may detach some of the nanoparticle-covering from the surface. As a result, thermal resistance decreases for the 0.1 % nanoparticle-coated micro-channel surface compared with the thermal resistance produced with 0.1 % nanofluids.

6 Conclusions

An experimental investigation was conducted on the thermal performance of a micro-channel surface used in a vapor chamber by using Cu-R141b nanofluid as the

Fig. 12 Heat flow density and thermal resistance comparison between bare microchannel/0.1 vol % Cu nanofluid and 0.1 vol % coated microchannel surface/pure R141b
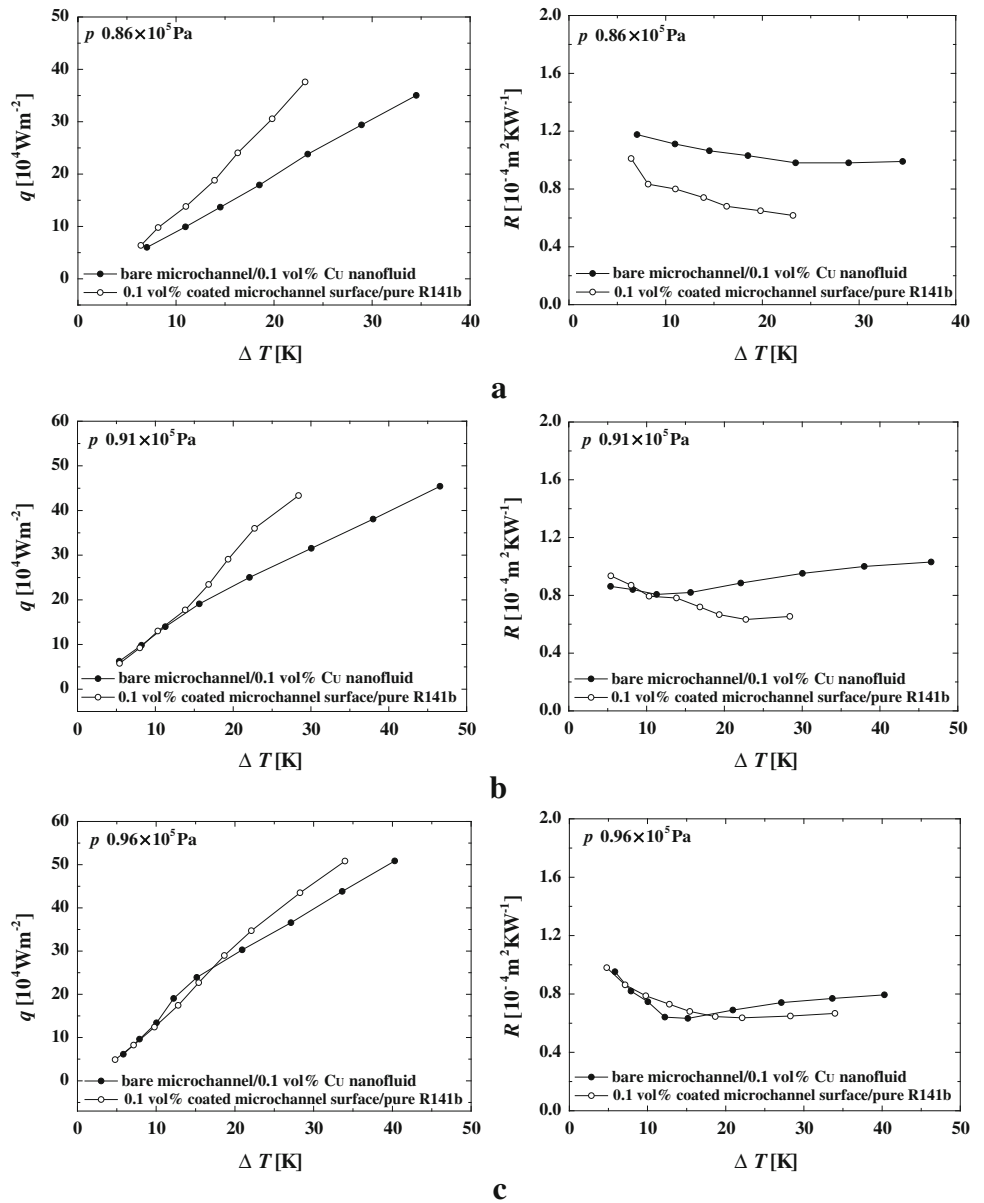
working fluid. A series of tests was conducted to investigate the heat transfer characteristic of nanoparticle deposition by using the base fluid of R141b. The conclusions obtained in this study can be summarized as follows:

1. The use of R141b-based Cu nanofluids with volume concentrations of 0.001 and 0.01 % as the working fluid could enhance the thermal performance of the micro-channel surface, especially under lower operating pressures that range from 0.86×10^5 Pa to 0.96×10^5 Pa. The working fluid with nanoparticles could enhance the thermal performance of the micro-channel surface because of the following reason: The nanoparticles deposited at the heat transfer surface and

formed a nanoparticle layer, thus extending the heat transfer area and increasing nucleation density to improve evaporation/boiling heat transfer. The extended heat transfer area and nucleation density increases simultaneously with increased nanoparticle concentration that could result in enhanced heat transfer effect. Optimal nanoparticle suspension was noted with 0.01 % volume concentration, which corresponds to minimum thermal resistance. Minimum thermal resistance is half that for R141b. Under some operating conditions, heat transfer deterioration was observed for nanofluid with 0.1 % volume concentration compared with R141b.

2. Operating pressure can significantly influence the heat transfer characteristic of micro-channel surface that
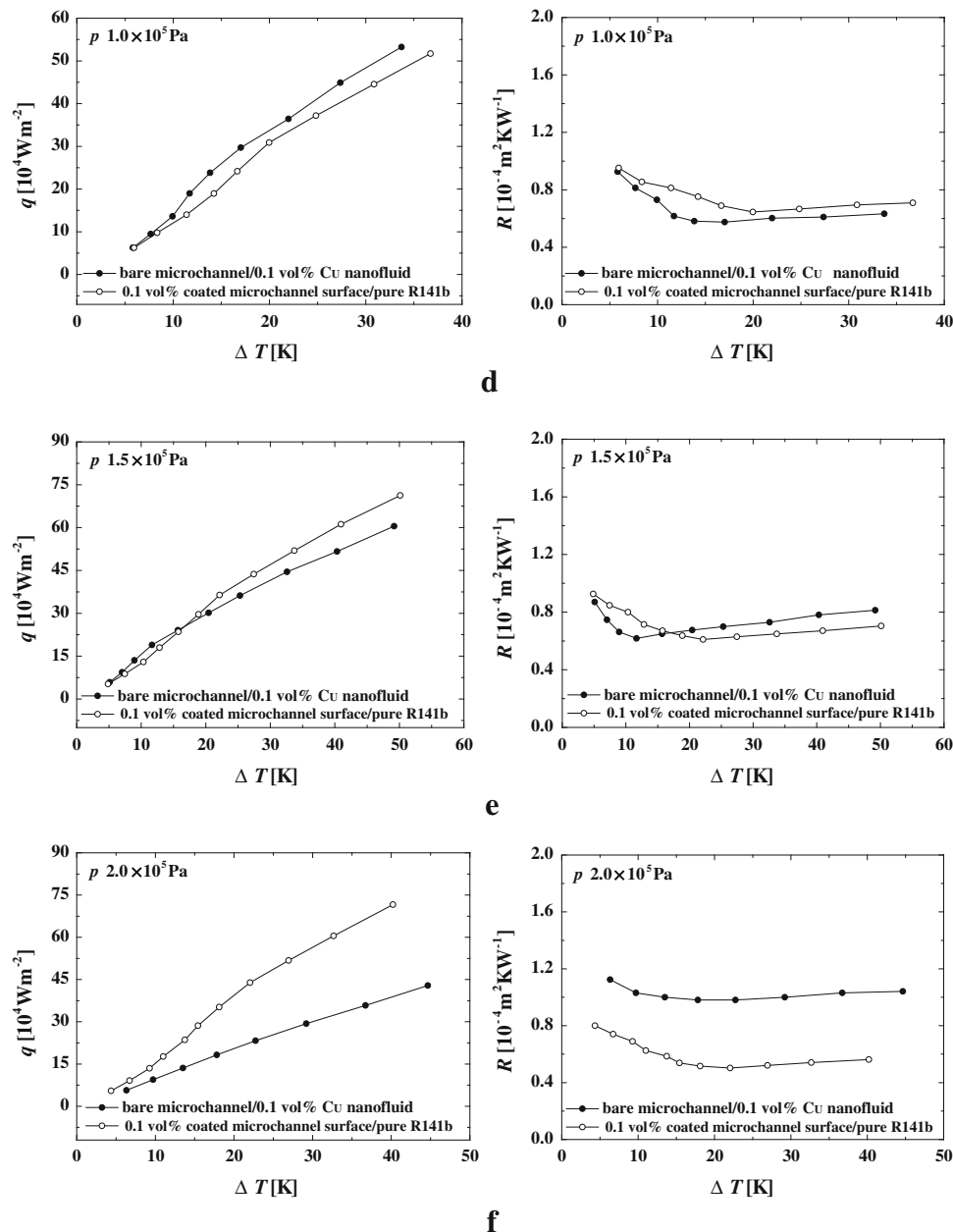
Fig. 12 continued

use nanofluids. The maximum reduction effect of the thermal resistance was 50 %, which corresponds to a 0.01 % volume concentration of nanofluid at low operating pressure. The following quantitative reasons may explain such occurrence: (1) The properties of the working fluids can be influenced by pressure. Increased pressure causes variation in working fluid surface tension and latent heat of vaporization; (2) Nucleation density, bubble dynamics, and contact angle on the boiling surface can be affected by pressure. The conjunct role of the above enhancement factor determines the influence of pressure on heat transfer

characteristics of nanofluids. The effect of thermal resistance of nanofluids for lower operating pressures is more apparent than that for higher operating pressures. A more evident deteriorating heat transfer effect is noted for the nanofluid with 0.1 % concentration compared with R141b at the operating pressure of 2.0×10^5 Pa.

3. Nanoparticle layers at the microchannel surface for nanofluids with different volume concentrations are observed. Experimental results for the thermal resistance of a nanoparticle deposition surface that used pure R141b showed that the formation of a

nanoparticle layer at the microchannel surface is the main reason for the improved thermal performance of the microchannel surface that used nanofluids.

References

1. Choi SUS (1995) Enhancing thermal conductivity of fluids with nanoparticles. ASME FED 231:99–105
2. Lee S, Choi SUS, Eastman JA (1995) Measuring thermal conductivity of fluids containing oxide nano-particles. Trans ASME 121:280–289
3. Choi SUS, Wang X, Xu W (1999) Thermal conductivity of nano-particle-fluid mixture. J Thermophys Heat Transfer 13(4):474–480
4. Xie H, Wang J, Xi T, Liu Y (2002) Thermal conductivity of suspensions containing nano-sized SiC Particles. Int J Thermophys 23(2):571–580
5. Xie X, Lee H, Youn W, Choi M (2003) Nano-fluids containing multiwalled carbon nano-tubes and their enhanced thermal conductivities. J Appl Phys 94(8):4967–4971
6. Choi SUS, Eastman JA, Li S, Yu W, Thompson J (2001) Anomalously increased effective thermal conductivities of ethylene glycol-based containing copper nano-particles. Appl Phys Lett 78(6):718–720
7. Das SK, Putra N, Thiesen P, Roetzel W (2003) Temperature dependence of thermal conductivity enhancement for nano-fluids. J Heat Transfer 125:567–574
8. Li CH, Peterson GP (2007) The effect of particle size on the effective thermal conductivity of Al_2O_3-water nanofluids. J Appl Phys 101:044312
9. Lee JH, Hwang KS, Jang SP, Lee BH, Kim JH, Choi SUS, Choi CJ (2008) Effective viscosities and thermal conductivities of aqueous nanofluids containinng low volume concnentrations of Al_2O_3 nanoparticles. Int J Heat Mass Transfer 51(11–12):2651–2656
10. Xuan Y, Li Q (2000) Heat transfer emhancement of nano-fluids. Int J Heat Fluid Flow 21(1):58–64
11. Xuan Y, Li Q (2003) Investigation on convective heat transfer and flow features of nano-fluids. J Heat Transfer 125:151–155
12. Fotukian SM, Esfahany MN (2010) Experimental study of turbulent convective heat transfer and pressure drop of dilute CuO/water nanofluid inside a circular tube. Int Commun Heat Mass Transf 37(2):214–219
13. Wang XQ, Mujumdar AS (2007) Heat transfer characteristics of nanofluids: a review. Int J Therm Sci 46(1):1–19
14. Vassallo P, Kumar R, D'Amico S (2004) Pool boiling heat transfer experiments in silica-water nano-fluids. Int J Heat Mass Transf 47(2):407–411
15. Das SK, Putra N, Roetzel W (2003) Pool boiling characteristics of nano-fluids. Int J Heat Mass Transfer 46(5):851–862
16. Kwark SM, Kumar R, Moreno G, Yoo J, You SM (2010) Pool boiling characteristics of low concentration nanofluids. Int J Heat Mass Transfer 53(5–6):972–981
17. Vassallo P, Kumar R, D'Amico S (2004) Pool boiling heat transfer experiments in silica-water nanofluids. Int J Heat Mass Transfer 47(2):407–411
18. Wen D, Ding Y (2005) Experimental investigation into the pool boiling heat transfer of aqueous based alumina nanofluids. J Nanopart Res 7:265–274
19. Kim S, Bang IC, Buongiorno J (2007) Surface wettability change during pool boiling of nanofluids and its effect on critical heat flux. Int J Heat Mass Transfer 45(7):4105–4116
20. Taylor RA, Phelan PE (2009) Pool boiling of nanofluids: comprehensive review of existing data and limited new data. Int J Heat Mass Transfer 52(23–24):5339–5347
21. White SB, Shih AJ, Pipe KP (2010) Effects of nanoparticle layering on nanofluid and base fluid pool boiling heat transfer from a horizontal surface under atmospheric pressure. J Appl Phys 107(11):114302–114307
22. Jeong YH, Chang WJ, Chang SH (2008) Wettability of heated surfaces under pool boiling using surfactant solutions and nanofluids. Int J Heat Mass Transfer 51(11–12):3025–3031
23. Suriyawong A, Wongwises S (2010) Nucleate pool boiling heat transfer characteristics of TiO_2-water nanofluids at very low concnentration. Exp Thermal Fluid Sci 34(8):992–999
24. Ahmed O, Hamed MS (2012) Experimental Investigation of the effect of particle deposition on pool boiling of nanofluids. Int J Heat Mass Transfer 55(13–14):3423–3436
25. Liu ZH (2010) Compositive effect of nanoparticle parameter on thermal performance of cylindrical micro-grooved heat pipe using nanofluids. Int J Therm Sci 500(4):558–568
26. Wei WC, Tsai SH, Yang SY, Kang SW (2005) Effect of nanofluid concentration on heat pipe thermal performance. IASME Trans 2:1432–1439
27. Kang SW, Wei WC, Yang SH (2006) Experimental investigation of silver nano-fluid on heat pipe thermal performance. Appl Therm Eng 26(17/18):2377–2382
28. Han WS, Rhi SH (2011) Thermal characteristics of Grooved Heat Pipe with hybrid nanofluids. Thermal Sci 15(1):195–206
29. Do KH, Ha HJ, Jang SP (2010) Thermal resistance of screen mesh wick heat pipes using the water-based Al_2O_3 nanofluids. Int J Heat Mass Transfer 53(25–26):5888–5894
30. Tsai CY, Chien HT, Ding PP, Chan B, Luh TY, Chen PH (2004) Effect of structural character of gold nanoparticles in nanofluids on heat pipe thermal performance. Mater Lett 58:1461–1465
31. [31] Chen YT, Wei WC, Kang SW, Yu CS (2008) Effect of nanofluids on flat heat pipe thermal performance. In: Proceedings of 24th IEEE semiconductor thermal measurement and management symposium. pp 16–20
32. Kang S, Wei W, Tsai S, Huang C (2009) Experimental investigation of nanofluids on sintered heat pipe thermal performance. Appl Therm Eng 29(5/6):973–979
33. Xue HS, Fan JR, Hu YC, Hong RH, Cen KF (2006) The interface effect of carbon nanotube suspension on the thermal performance of a two-phase closed thermosyphon. J Appl Phys 100(10):104909
34. Noie SH, Heris SZ, Kahani M, Nowee SM (2009) Heat transfer enhancement using Al_2O_3/water nanofluid in a two-phase closed thermosyphon. Int J Heat Mass Transfer 52(30):700–705
35. Huminic G, Huminic A, Morjan I, Dumitrache F (2010) Experimental study of the thermal performance of thermosyphon heat pipe using iron oxide nanoparticles. Int J Heat Mass Transfer 54(1–3):656–661
36. Qu J, Wu HY, Cheng P (2010) Thermal performance of an oscillating heat pipe with Al_2O_3-water nanofluids. Int Commun Heat Mass Transf 37(2):111–115
37. Ma HB, Wilson C, Borgmeyer B, Park K, Yu Q, Choi SUS, Triumala M (2006) Effect of nanofluid on the heat transport capability in an oscillating heat pipe. Appl Phys Lett 88(14):143116
38. Ma HB, Wilson C, Park K, Choi SUS, Tirumala T (2006) An experimental investigation of heat transport capability in a nanofluids oscillating heat pipe. J Heat Transfer 128(11):1213–1216
39. Do KH, Jang SP (2010) Effect of nanofluids on the thermal performance of a flat micro heat pipe with a rectangular grooved wick. Int J Heat Mass Transfer 53:2183–2192
40. Diao YH, Liu JR, Zhao YH (2009) An experimental investigation on heat transfer characteristics for micro-capillary evaporator. Exp Heat Transfer 22(2):87–98